

Article

Spatial–Temporal Patterns of Historical, Near-Term, and Projected Drought in the Conterminous United States

Susan M. Kotikot ¹  and Olufemi A. Omitaomu ^{2,*} ¹ Department of Geography, Pennsylvania State University, University Park, PA 16802, USA; smk6598@psu.edu² Computational Sciences and Engineering Division, Oak Ridge National Laboratory, Oak Ridge, TN 37831, USA

* Correspondence: omitaomuoa@ornl.gov

Abstract: Major droughts in the United States have heavily impacted the hydrologic system, negatively effecting energy and food production. Improved understanding of historical drought is critical for accurate forecasts. Data from global climate models (GCMs), commonly used to assess drought, cannot effectively evaluate local patterns because of their low spatial scale. This research leverages downscaled (~4 km grid spacing) temperature and precipitation estimates from nine GCMs' data under the business-as-usual scenario (Representative Concentration Pathway 8.5) to examine drought patterns. Drought severity is estimated using the Palmer Drought Severity Index (PDSI) with the Thornthwaite evapotranspiration method. The specific objectives were (1) To reproduce historical (1966–2005) drought and calculate near-term to future (2011–2050) drought patterns over the conterminous USA. (2) To uncover the local variability of spatial drought patterns in California between 2012 and 2018 using a network-based approach. Our estimates of land proportions affected by drought agree with the known historical drought events of the mid-1960s, late 1970s to early 1980s, early 2000s, and between 2012 and 2015. Network analysis showed heterogeneity in spatial drought patterns in California, indicating local variability of drought occurrence. The high spatial scale at which the analysis was performed allowed us to uncover significant local differences in drought patterns. This is critical for highlighting possible weak systems that could inform adaptation strategies such as in the energy and agricultural sectors.

Keywords: drought assessment; PDSI; USA; downscaled climate data; spatial temporal

Citation: Kotikot, S.M.; Omitaomu, O.A. Spatial–Temporal Patterns of Historical, Near-Term, and Projected Drought in the Conterminous United States. *Hydrology* **2021**, *8*, 136. <https://doi.org/10.3390/hydrology8030136>

Academic Editor: Nicholas Dercas

Received: 8 August 2021

Accepted: 4 September 2021

Published: 8 September 2021

Publisher's Note: MDPI stays neutral with regard to jurisdictional claims in published maps and institutional affiliations.



Copyright: © 2021 by the authors. Licensee MDPI, Basel, Switzerland. This article is an open access article distributed under the terms and conditions of the Creative Commons Attribution (CC BY) license (<https://creativecommons.org/licenses/by/4.0/>).

1. Introduction

In the United States, significant historical drought events have had devastating effects on the hydrologic system, accordingly impacting energy generation and production [1,2], agriculture [3,4], water availability and associated infrastructure [5], and green infrastructure and vegetation health [6]. Inevitably, the national economy has suffered the ultimate socioeconomic consequence. Understanding the spatial–temporal characteristics of drought onset is important in estimating probable propagation, spatially into nearby regions and progression to other dimensional categories [7]. It has been shown that drought conditions may, with time, extend to surrounding regions of similar climate patterns [8]. This will generally depend on the existing teleconnections of the climate regions in question. Determination of existing climate networks in a region is a good strategy for analyzing possible paths of spatial propagation thereby augmenting projections of drought to surrounding areas.

The topic of drought has been extensively studied, e.g., in [9,10], normally with the desire to gain more understanding to enable forecasting of future events and hence better preparedness. Nevertheless, there exists considerable disagreement as to a comprehensive definition of drought [11]. Many researchers refer to drought as being associated with a prolonged and abnormal moisture deficiency [12]. The cause or consequence of the deficiency translates to different categories of drought, which include meteorological,

hydrological, agricultural, and socioeconomic. Some authors [12] have recommended separate examination of drought by category. However, it is not easy to clearly isolate the categories as the boundary separating them is often vague [13]. The creeping nature of drought makes it difficult to predict its onset or ending. It gradually develops, cumulatively contributing to its severity. Tannehill for example, noted that the first day of a drought is as important as the last; however, we only become aware of its progression when the effects start to show [14].

The mitigation of drought effects depends on the availability and accuracy of information on the probability of occurrence, the intensity of drought, its frequency, and duration. There are tools developed specifically for monitoring and predicting drought. In the United States, the U.S. Drought Monitor serves as the primary resource for drought assessment, providing historical records and near-real-time estimates expressed in various severity indices including PDSI and SPI. Other resources providing specific aspects of drought include Climate Engine, Drought-ACIS, CRN Soil Moisture and Temperature, Drought Risk Atlas, and Drought Management Database, among others. Elsewhere, tools dedicated to drought assessment have also been developed [15]. Often, scientists strive to establish societal resiliency to the impacts of drought through research. Improved understanding of the climate system has specifically enabled modeling approaches that simulate the climate system, making it possible to create different outcome scenarios. Using data from various GCMs, researchers have attempted to estimate future drought events using models calibrated based on known historical events [16,17]. Others have utilized ground observation data to derive and study drought patterns [18], and others have used observation in combination with GCM data [19]. While the estimates are useful in assessing regional drought, it is not easy to evaluate local patterns mostly because GCM data are at the moderate to low spatial scale, and observation stations are sparse.

Recent developments in climate studies have included the permeation of network analysis for its analytical ability to uncover unique local to global properties of the climate [20]. The concept was first introduced in [21] and is based on measured pairwise interactions between climates of different locations. Applications in drought studies have involved the identification of the drought tolerance and susceptibility of different cultivars, predictive modeling, comparing climate dynamics in different locations [22,23], and reducing the dimensionality of large climate data [24], among other things. Network analysis has been used to expose both local and global variability in climate as measured by variables such as mean temperature and precipitation. Further, it allows for the division of large areas into clusters using community detection algorithms that evaluate similarity metrics between climate locations based on a characteristic climate variable, in this case, PDSI time series. Climate locations are grouped into clusters based on the calculated similarity measure. The division is such that, in each cluster, the fluctuations of a climate variable are in phase [22] or have similar response to physical processes such as the El Niño–Southern Oscillation (ENSO) [25]. Limited studies have investigated the existence of community structure within local, state, or watershed levels. Many authors have studied the networks at national, regional [26], and global [27,28] scales. Often, interesting patterns are uncovered that explain climate phenomenon that cannot be explained through conventional approaches.

The main goal of the current research was to understand the spatial–temporal patterns of drought in the United States. First, we inspected and presented the historical droughts as determined from nine GCMs' data while verifying with known drought events. Second, we estimated near-term to future drought patterns. In both cases, we determined the general trends in the proportion of land areas affected by drought. We then examined the spatial occurrence of severe drought at decadal time scales to enable comparison among GCM data and geographically assess past and potential drought. Lastly, we employed the network-based approach to determine potential networks associated with the occurrence of drought as measured using PDSI. The research is novel in that (1) it examines drought, a critical topic to the socioeconomic development of the United States; (2) it performs the assessment at a high spatial resolution that has not been attempted before at a national

level, thus revealing unique local structure and utility for localized drought assessment that is not possible with coarse GCM data; (3) it employs an innovative network-based approach to reveal and characterize coherent subsystems within the state of California during a typically dry spell and demonstrates local drought patterns; and (4) it cross compares findings among nine GCMs' data presenting a comprehensive analysis.

2. Materials and Methods

We quantified historical and future drought severity using the Palmer Drought Severity Index (PDSI). The PDSI was developed by Palmer [29] and is an extensively used method for quantifying drought severity. To compute PDSI, temperature, precipitation, and available water capacity data are required. The analysis utilized a time series (1966–2005 and 2011–2050) of downscaled monthly temperature and precipitation data generated by Naz et al. from nine GCMs following downscaling procedures described in [30]. Our focus on RCP 8.5 was to indicate probable drought conditions if emissions continue unabated. In the downscaling procedure, coarser resolution GCM outputs from the Coupled Model Intercomparison Project, phase 5 (CMIP5), GCMs under Representative Concentration Pathway (RCP) 8.5 were first dynamically downscaled to 18 km using the RegCM4 model. The RegCM4 model outputs were then statistically bias corrected using observations from the Parameter-elevation Regressions on Independent Slopes Model (PRISM) to obtain data at approximately 1/24 degrees (~4 km) resolution. Available water capacity (AWC) data at the top 100 cm were obtained from the USDA State Soil Geographic Database (STATSGO). Table 1 shows the GCM data properties used in this study.

Table 1. GCM data properties used in this study.

| Model | Center | AtmRes | VL in Atm | Model Components | | | | | | | |
|--------------|--|-----------|-----------|------------------|---|---|---|---|---|---|---|
| | | | | a | b | c | d | e | f | g | |
| ACCESS1-0 | Commonwealth Scientific and Industrial Research Organization and Bureau of Meteorology, Australia | 1.25*1.88 | 38 | ✓ | ✓ | | ✓ | | | | ✓ |
| BCC-CSM1-1 | Beijing Climate Center, China | 2.79*2.81 | 26 | ✓ | ✓ | | ✓ | ✓ | ✓ | ✓ | ✓ |
| CCSM4 | National Center for atmospheric Research, USA | 0.94*1.25 | 26 | ✓ | ✓ | | ✓ | ✓ | | | ✓ |
| CMCC-CM | Centro Euro-Mediterraneo sui Cambiamenti Climatici Climate | 0.75*0.75 | 31 | ✓ | ✓ | | | ✓ | | | ✓ |
| FGOALS-g2 | State Key Laboratory Numerical Modeling for atmospheric Sciences and Geophysical Fluid Dynamics (LASG)—Institute of Atmospheric Physics, China | 1.66*2.81 | 26 | ✓ | ✓ | | ✓ | ✓ | ✓ | ✓ | ✓ |
| MPI-ESM-MR | Max Planck Institute Earth System Model | 1.87*1.88 | 95 | ✓ | ✓ | | ✓ | ✓ | ✓ | ✓ | ✓ |
| MRI-CGCM3 | Meteorological Research Institute, Japan | 1.12*1.13 | 48 | ✓ | ✓ | | ✓ | ✓ | | | ✓ |
| NorESM1-M | Norwegian Earth System Model | 1.89*2.5 | 26 | ✓ | ✓ | ✓ | ✓ | ✓ | | | ✓ |
| IPSL-CM5A-LR | Institut Pierre Simon Laplace | 1.89*3.75 | 39 | ✓ | ✓ | | ✓ | ✓ | ✓ | ✓ | ✓ |

AtmRes—atmospheric resolution, VL in Atm—vertical levels in atmosphere, a—atmosphere, b—aerosol, c—atmospheric chemistry, d—land surface, e—ocean, f—ocean-biogeochem, g—sea ice.

2.1. PDSI Computation

The PDSI is a meteorological index that is a measure of the departure of moisture supply and is based on the supply and demand concept of the water balance. It allows comparison of drought severity across time and space by standardizing measurement of moisture conditions. PDSI was computed for each month, separately for the historical and projected periods at ~4 km grid spacing using the MATLAB tool developed by Jacobi et al. [31] and utilizing the Thornthwaite's evapotranspiration method [32] to estimate

climate moisture demand. A detailed description of the PDSI calculation can be found in Palmer [29].

In summary, the computation procedure begins with a hydrologic accounting using a water balance method, which incorporates preceding and prevailing meteorological conditions of an area including soil moisture, moisture supply, and demand (evapotranspiration) to determine continued normalcy of climate conditions. Soil moisture is handled by dividing the soil layer into two layers in a model with the following assumptions:

- Evapotranspiration (ET) losses from the soil occur if potential evapotranspiration (PE) > precipitation (P) for the month.
- The surface layer (L_s) contains 1 inch of the available moisture at field capacity.
- The underlying layer (L_u) has an available capacity that depends on soil characteristics and the depth of the effective root zone.
- Moisture can only be removed from L_u after available moisture from L_s is all removed.
- Recharge to L_u can only occur after L_s has been brought to field capacity.
- ET losses from L_s occur at the potential rate.
- Losses from L_u depend on the depth of the effective root zone, initial moisture content in L_u , PE, and the combined AWC in both soil layers.
- Runoff occurs only if both layers reach their combined field capacity.

For each month, the Climatologically Appropriate for Existing Conditions (CAFEC) precipitation, P^* , is then calculated. It is the amount of precipitation required to maintain the climate of an area at normal moisture conditions. The difference, d , between the actual precipitation, P , and the CAFEC precipitation, P^* , is then calculated and represents the monthly departure of P from P^* , and thus the departure from average moisture climate of the region. The departures, d , must be weighted to develop comparable indices of moisture across time and space. A weighting factor, K_j , is therefore developed that transforms the departures according to their apparent significance to the local weather and climate. An index of abnormality, $Z = K_j d$, is then developed for prolonged drought periods by combining the moisture anomaly indices. Controlling for rapid changes in month-to-month PDSI, it is defined as a weighted sum of the preceding PDSI and contemporaneous Z value. Drought severity for the i th month, $X(i)$, is established as in Equation (1).

$$X(i) = 0.897x(i-1) + Z(i)/3 \quad (1)$$

2.2. Spatial–Temporal Analysis

Temporal patterns were summarized by determining the percentage land area under abnormally dry (−1.0 to −1.9), moderate drought (−2.0 to −2.9) and severe drought (<−3.0) conditions. This provided an overview of the extent of drought conditions while comparing among the models. The desire was to capture and verify significant past droughts as well as identify potential future droughts.

For each grid cell at ~4 km spacing, the computed PDSI values were then analyzed to uncover spatial–temporal patterns. First, PDSI values were summarized into a single value, representing the average value of the summer months (June, July, August) for each year. Here, we focused on only summer months because of known differences in PDSI between winter and summer months that would influence computed averages. For example, the Thornthwaite evapotranspiration approach used in the study is overly dependent on temperature, yet other factors such as solar radiation, wind speed, and water vapor pressure deficit have greater influence on PET [33]. It has also been found that PDSI in the U.S. great plains is mostly influenced by moisture supply, yet PDSI does not account for delayed runoff from ice and snow that occurs in winter but assumes that precipitation is immediately available [34]. The Mann–Kendall [35] trend test was then performed to detect for the presence of a monotonic trend in the annual average summer PDSI. Monotonic trends imply a consistent gradual change in one direction. Because this is a non-parametric trend test, the expectation is that possible outliers or non-normality will not significantly affect the test result [36]. The null hypothesis is that the data were generated

through an independent random process and, therefore, are uniformly distributed, while the alternative hypothesis is that the data exhibit a monotonic trend [37]. In this case, the interest was to determine whether there is any increasing or decreasing trend in PDSI. The trends can be interpreted in relation to the dry or wet conditions.

The Mann–Kendall trend test only tests for the presence of a monotonic trend but does not quantify it. Sen slope [38,39] has been recommended and widely used to quantify a monotonic trend by calculating among other things, the slope as a linear rate of change. The quantity represents the median slope joining all pairs of observations measured in quantity per unit time. In this case, values are average change in PDSI per year for the summer months.

Spatial patterns were further summarized by calculating, for each decade of the historical and projected periods, the average number of severe drought months per year. This indicated the spatial occurrence of severe drought across USA, highlighting severely affected areas as decadal aggregates.

2.3. Local Spatial Heterogeneity

We used a network analysis approach to investigate the spatial–temporal heterogeneity of PDSI for California between 2012 and 2018. This was to reveal independent local microclimates as indicated by similarities or differences in historical patterns of dryness or wetness between different locations, demonstrating the utility of high-spatial-resolution climate data for localized drought assessment. In the approach, grid points at ~4 km spacing on a latitude and longitude space were randomly sampled and considered as vertices with PDSI as the attribute. A 3-month moving average was performed on the PDSI time series data to smooth out interim variations and feature longer-term trends. The vertices were joined by edges defined as statistical correlation between vertex attributes (PDSI). These correlations were used to weight the edges. Existing networks were delineated through a pruning method that eliminated edges with weak correlations based on a predetermined threshold. Initially, correlations were computed for all possible combinations of vertices resulting in a perfectly connected network. Weak edges were eliminated by selecting only correlation coefficients ≥ 0.9 that were statistically significant at 99% confidence level. Previous authors have considered values of ≥ 0.5 [40] and ≥ 0.9 with p -values of very high significance [41]. We preferred the Pearson correlation coefficient as a measure of link strength because of its simplicity. Non-linear measures such as mutual information have been studied before and found to be significantly comparable to the Pearson coefficient [42]. Nevertheless, future work should examine other non-linear measures to capture any non-linear relationships. It is suggested that time series values should be normalized to reduce seasonality, which might amplify correlations [43]. In this analysis, PDSI values were not normalized before network creation because PDSI is itself an index of the climate that is generated by considering deviations from normal conditions. Spatial autocorrelation was not an issue here since the geographic location of vertices was not considered in the statistical correlation and network creating stages. However, a test of temporal autocorrelation was performed, and the results indicated no autocorrelation.

The goal here was to delineate existing local subregions (communities) exhibiting similar properties as measured by time series PDSI. Communities were extracted based on some degree of internal cohesion among the vertices, in this case, the Pearson correlation coefficient. Beginning with a network where the Pearson correlation coefficients between vertex pairs were greater than 0.9, the popular modularity function of Newman and Girvan [44] was used as a quantitative measure to evaluate partitions for those that displayed a genuine network structure. For a given division of a network's nodes, modularity reflects the concentration of edges within the division compared to the random distribution of edges in a perfectly connected network. Considering a pair of nodes (i, j) in a network with n nodes and m edges, the network may be partitioned into two clusters using a membership variable, s , such that $s_i = 1$ if node i belongs to cluster 1 or $s_i = -1$ if node i belongs to cluster 2. If the adjacency matrix of the network is A , $A_{ij} = 0$ if there is no interaction

between i and j , and $A_{ij} = 1$ if there is interaction. Modularity, Q , is then defined as the fraction of edges that fall within group 1 or 2, minus the expected number of edges within groups 1 and 2 for a random graph with the same node degree distribution as the given network. This algorithm is illustrated in Equation (2).

$$Q = \frac{1}{2m} \sum_{i,j} \left(A_{ij} - \frac{k_i h_j}{2m} \delta(C_i, C_j) \right), \quad (2)$$

where m is the total number of edges of the graph, A is the adjacency matrix, A_{ij} is the weight of the edge between i and j , k_i is the degree of vertex i , and the sum runs over all vertex pairs. The δ function is 1 if i and j belong to the same community and 0 otherwise.

Using the modularity optimization algorithm of Blondel et al. [45], communities were extracted such that modularity within the communities was a maximum. The algorithm involves a two-phase approach, in which, in the first phase, each node is placed in its own community. Nodes are then paired and the gain in modularity is estimated for moving any node to a different community. The process is repeated for all nodes until no further gain in modularity is detected. In the second phase, the identified communities are used as nodes to iterate the previous operation until maximum modularity is gained. The partitioning process is summarized in Figure 1.

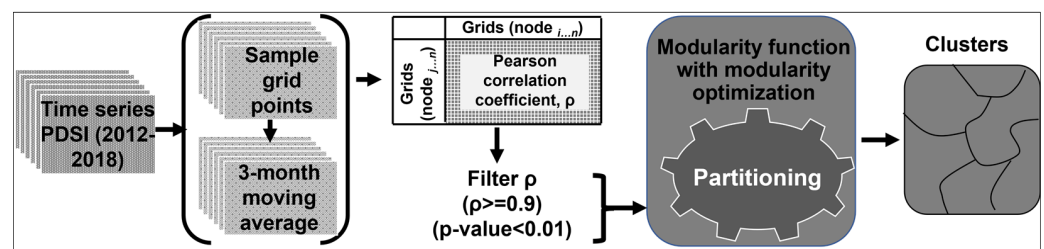


Figure 1. Processing workflow for network analysis clusters partitioning process.

3. Results

The results for the conterminous USA and some regional case studies are presented in this section.

3.1. Temporal Patterns

Figure 2 shows the proportions of conterminous USA land area under abnormally dry (PDSI between -1.0 and -1.9), moderate (PDSI between -2.0 and -2.9), and severe (PDSI of -3.0 and less) drought for the historical (1966–2005) and near-term to projected periods (2011–2050). The three severity categories referenced here were derived as used in the Drought Monitor of the National Drought Mitigation Center at the University of Nebraska–Lincoln. There is low comparison of results among the models for both periods. However, comparable results were observed between selected models for specific periods of time. During the historical period, NorESM, ACCESS, BCC, CCSM4, and FGOALS indicated the prevalence of severe drought during 1966 to 1968. ACCESS and BCC showed the prevalence of severe drought between 2002 and 2005. MRI, NorESM, CMCC, and FGOALS indicated extensive severe droughts between 2000 and 2003. Four models (BCC, CCSM4, CMCC, FGOALS) indicated extensive severe drought within the near-term period 2011–2015, while MPI, NorESM, IPSL, ACCESS, and MPI indicated considerable severe and moderate drought within the same period. IPSL, ACCESS, CMCC, and MPI indicated increased severe drought in the years approaching and including 2050.

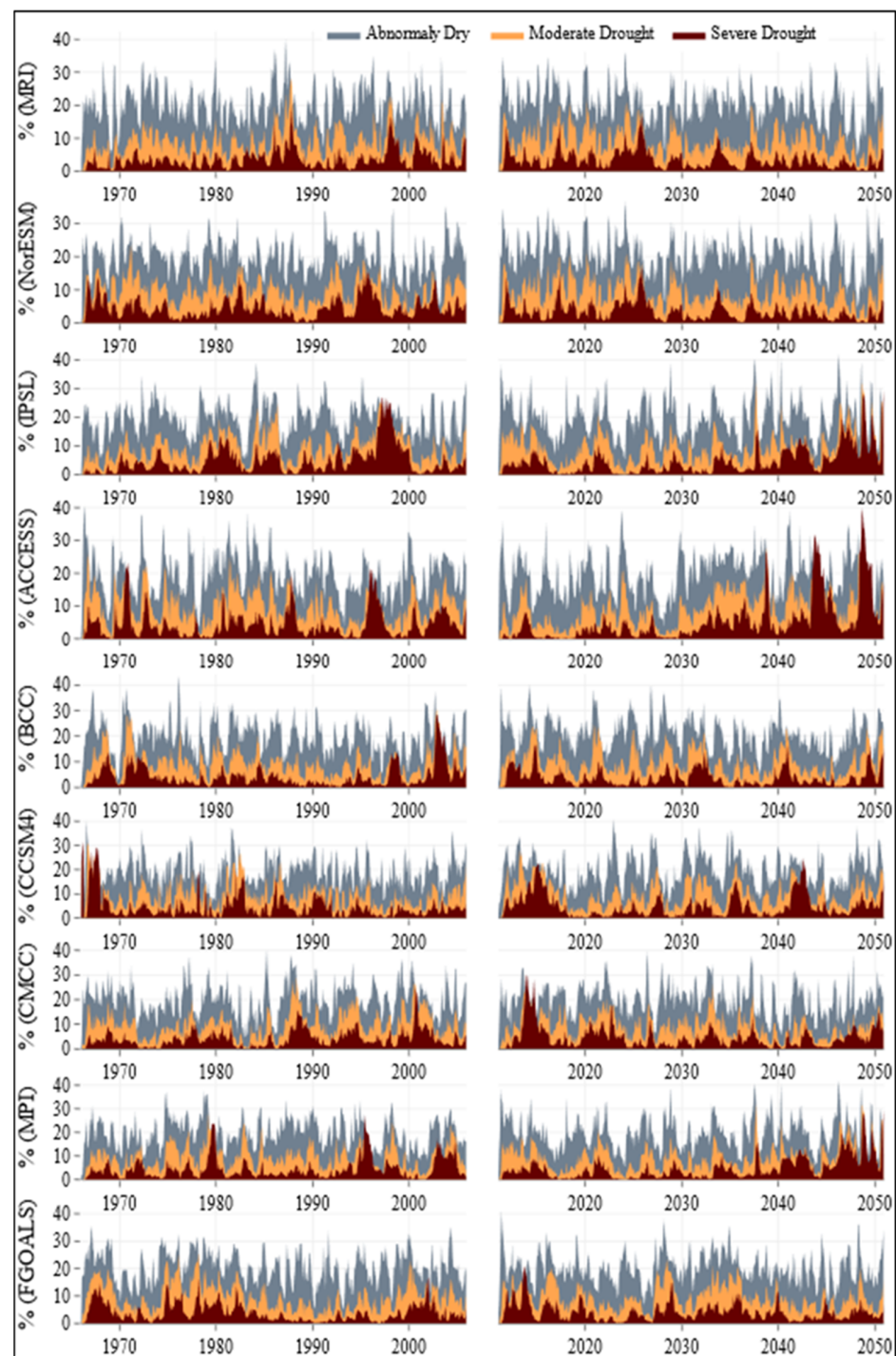


Figure 2. Proportion of conterminous USA land area under drought. The left panel represents the historical period, and the right panel represents the future period.

The historical period is characterized by cyclic patterns of moderate and severe drought with no clear uptrends or downtrends. In the near-term to projected period, some models (MRI, FGOALS) showed a downtrend and some (IPSL, ACCESS, MPI) showed uptrends in drought occurrences. These trends can generally be inferred from Figure 2, more clearly for moderate and severe drought categories. Figure 3a,b illustrates the trend of severe droughts only ($PDSI < -2.9$). There is a general agreement among most models of high proportions of USA land area being under severe drought between the periods

1966–1968, 1969–1972, 1995, 2012–2018, and 2048–2050. No definitive trend can be described comparatively for all the models.

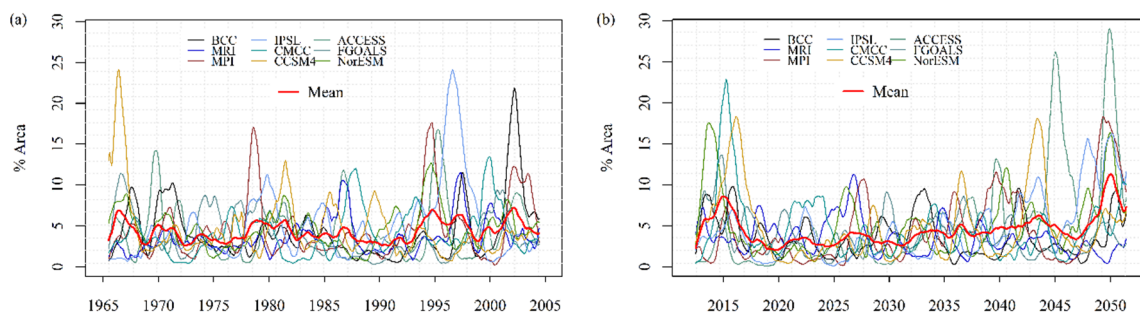


Figure 3. Proportion of conterminous USA land area under severe drought for (a) historical and (b) projected periods.

3.2. Spatial–Temporal Patterns

Considerable differences in the spatial–temporal occurrence of drought over the CONUS are observed among the nine models used in this study. However, over the historical period (Figure 4a), the models indicate a similar drying trend for parts of southwestern CONUS extending southern California, southern Nevada, and western Arizona. The region exhibits most rapid drying in the CONUS for the studied period. In other parts of the country, slow drying or wetting was observed, with minimal spatial similarity among the models. At least two to three models indicate a corresponding trend for specific regions. Relative to the historical period, the projected spatial–temporal trends (Figure 4b) show elevated gradients of drying for southwestern CONUS from ACCESS, CCSM4, CMCC, FGOALS, IPSL, MPI, and NorESM models. BCC and MRI models show slow drying and wetting for most parts of CONUS. Again, the projected spatial–temporal patterns are unmatched among most models for most parts of the country. Even so, a subset of the models show similar trends for specific areas. For example, CCSM4, CMCC, IPSL, MPI, and NorESM show drying in south Florida.

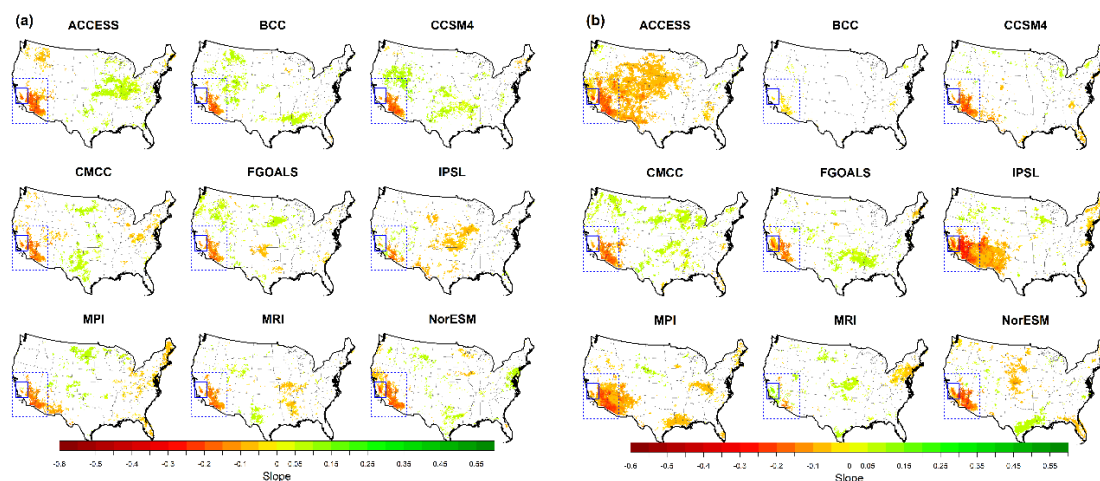


Figure 4. Spatial–temporal trends of drought occurrence for the historical (a) and projected periods (b). Dotted blue box shows a region of comparable trend among the models. The solid black box shows a small, isolated region in middle California.

Figure 5a shows the average number of months per year that experienced severe drought within the indicated ten-year period. Each row in the figure shows results for a single model. Between 1966 and 1975, there is minimal agreement among the models regarding the spatial occurrence of severe drought. With ACCESS showing widespread severe drought in most parts of the country, the other models show intense drought mostly in the mid-west region and zero to at most two months per year in other parts.

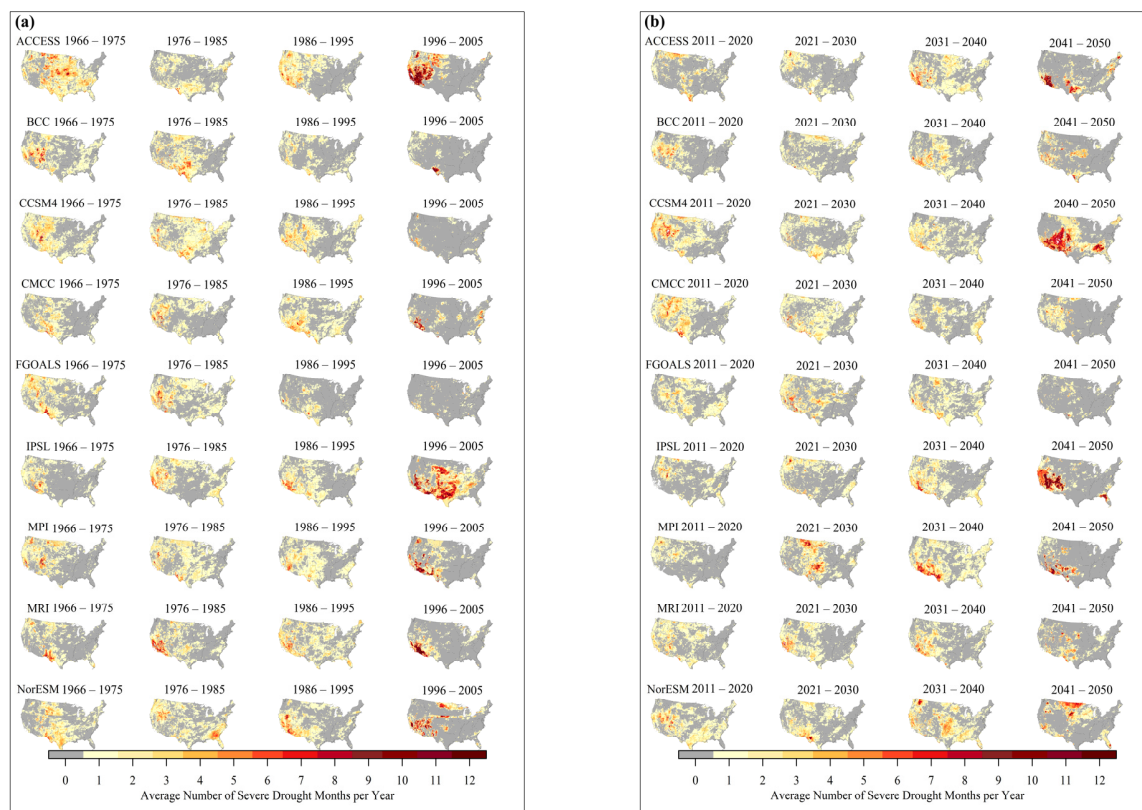


Figure 5. The spatial occurrence of severe droughts in decadal time periods for the historical (a) and projected (b) periods. Each map in the figure shows the average number of severe drought months per year for the indicated decade.

In 1976–1985, ACCESS, BCC, and CCSM show extensive severe drought in Texas while CCSM, CMCC, FGOALS, IPSL, and MRI show the same in western USA. Except for BCC and FGOALS that show patches of severe drought, the other models show diffuse severe droughts in the mid to western regions of the country between 1986 and 1995. Intra-model differences are indicative of the geography of severe droughts that were experienced for the specified periods. BCC, CCSM4, CMCC, and FGOALS all show less severe drought between 1996 and 2005 except for very few intense patches. ACCESS and IPSL show widespread and frequent spells of drought while MPI, MRI, and NorESM show smaller patches of frequent severe drought in southeastern USA. Some regions of the country, such as California, have had consistent cycles of severe drought through at least two of the four decadal time periods. IPSL and MRI show intense drought in southern California and Arizona between 1976 and 2005.

In the near-term period of 2011–2020, most models show severe droughts in western USA (Figure 5b). In 2021–2030, models considerably disagree on the spatial patterns of potential severe drought occurrence. Particularly conspicuous is BCC showing extensive and protracted severe drought in middle and northern USA. Between 2031 and 2040, all the models show expectation of extended cycles of severe drought in western USA and scattered areas of at most three months per year on average, of severe drought. Within the decade, all the models indicate that large parts of California will experience extended severe drought. In the decade, 2041–2050, ACCESS, CCSM4, IPSL, and NorESM indicate severe droughts extending 6 to 12 months per year in varied parts of USA. Scattered patches of less extended severe droughts are shown in BCC, MPI, CMCC, and MRI, with FGOALS showing the least expectation of severe drought. Spatially, affected areas are expected to change moving forward from 2011 to 2050. There is little geographical consistency in the frequency of severe drought occurrences—drought in one location does not advance into the next decade. However, there are small areas where, according to some models, severe drought is extending through at least two decades. ACCESS, CCSM4, IPSL, and MPI show

recurrent severe drought in the southern parts of California, Arizona, and New Mexico in the 2030s through to the 2040s.

3.3. Spatial Patterns of Local Heterogeneity

Climate networks constructed for California revealed the clusters in Figure 6. These clusters delineate regions that are similar in terms of temporal occurrence of drought between 2012 and 2018 as measured by PDSI. At least seven clusters can clearly be identified in all the models. These do not all spatially match among the models. However, there are specific clusters (labeled with similar numbers in Figure 5) that are identical among several models. The spatial extent of cluster 1 in Figure 6 seems nearly identical for NorESM, BCC, CCSM4, and MRI, with majority of the nodes roughly overlaying among all the models apart from CMCC where some nodes are in a different spatial location. Nodes in cluster 2 take a similar spatial pattern in MRI and ACCESS, partly matching those in CCSM4, CMCC, and MPI. In middle California, nodes in cluster 3 assume a nearly perfect shape for BCC, CMCC, and MRI. A group of nodes within the same spatial extent are in the same cluster in FGOALS and IPSL, though not within a clearly defined boundary. Other large clusters share a significant number of nodes among the models, signifying the presence of a unique community structure.

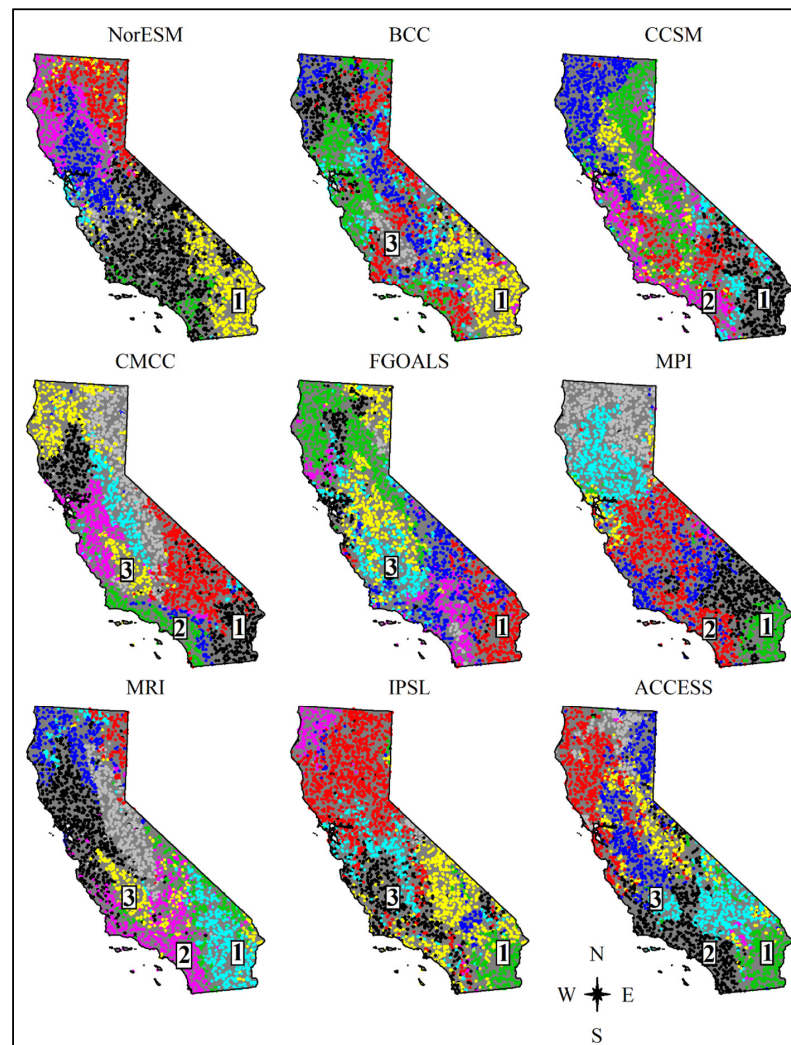


Figure 6. Network-based clusters illustrating spatial temporal heterogeneity of drought in California, USA as measured using time series PDSI for the period 2012–2018. The colors are only used here to show the presence of clusters. The colors do not indicate similar clusters across models. Number labels are used to show clusters with similar spatial extents among models.

In Table 2, we describe the topology of the constructed network from which the community structure in Figure 6 was derived. In all the models (except IPSL), the network density does not exceed 5%. This low density indicates heterogeneous spatial–temporal patterns of drought in California between 2012 and 2018. Global clustering coefficients of 0.5 show evidence of node clustering, affirming the heterogeneity of spatial–temporal drought in California within the referenced period. Apart from one model, CCSM4, with a modularity of 0.4, all other models attained a modularity of 0.5 and greater. This shows that the connections between nodes within a cluster are stronger than connections between nodes in the cluster with those outside the cluster, and that the number of connections within a cluster are more than would be expected by random chance.

Table 2. Topology characteristics of the PDSI-based network.

| | Models | Clustering Coefficient | Density | Modularity |
|----|--------|------------------------|---------|------------|
| 1. | CCSM4 | 0.5665 | 0.0432 | 0.4142 |
| 2. | ACCESS | 0.5554 | 0.0238 | 0.6118 |
| 3. | BCC | 0.5653 | 0.0323 | 0.6334 |
| 4. | CMCC | 0.5707 | 0.0117 | 0.7633 |
| 5. | FGOALS | 0.5244 | 0.0195 | 0.5943 |
| 6. | IPSL | 0.5964 | 0.0547 | 0.5115 |
| 7. | MPI | 0.5627 | 0.0208 | 0.7274 |
| 8. | MRI | 0.5601 | 0.0242 | 0.6629 |
| 9. | NorESM | 0.5686 | 0.0314 | 0.6267 |

4. Discussions

Numerous studies on global drought patterns have been carried out utilizing GCM data. General discrepancies in estimated drought trends among models have been confirmed and attributed to differences in applied methodologies [46–48], including variation in calibration periods and forcing data characteristics. The current paper provides an assessment of drought as measured using the PDSI. PDSI is one among many indices of defining drought and remains the most widely used in the United States. It integrates a comprehensive hydrologic accounting rather than providing statistics on individual aspects of the climate such as precipitation and soil moisture.

Our PDSI outputs compared fairly with those presented in [49,50] for the historical period of 1966–1995 but differed considerably for the period 1996–2005. We must mention that while our PDSI values were computed based on monthly GCM data at ~0.04 degrees spatial resolution, PDSI by Dai were computed based on observed climate data at ~2.4 degrees spatial resolution. Obtained root mean square error (RMSE) and mean absolute error (MAE) are shown in Table 3. With our outputs as the simulated data set, RMSEs between 2 and 3 were obtained for three out of four of the tested decadal time steps.

Table 3. RMSE and MAE of our PDSI with PDSI outputs of Dai [50].

| | | ACCESS | BCC | CCSM4 | CMCC | FGOALS | IPSL | MPI | MRI | NorESM |
|------|----|--------|-------|-------|-------|--------|-------|-------|-------|--------|
| RMSE | p1 | 2.90 | 2.99 | 2.94 | 2.76 | 2.98 | 2.80 | 2.87 | 2.80 | 2.90 |
| | p2 | 3.36 | 3.39 | 3.20 | 3.05 | 3.41 | 3.45 | 3.31 | 3.36 | 3.45 |
| | p3 | 3.33 | 3.23 | 3.39 | 3.44 | 3.51 | 3.49 | 3.41 | 3.48 | 3.49 |
| | p4 | 20.13 | 20.16 | 20.13 | 20.10 | 20.12 | 20.19 | 20.14 | 20.13 | 20.14 |
| MAE | p1 | 2.33 | 2.39 | 2.33 | 2.22 | 2.39 | 2.24 | 2.30 | 2.24 | 2.34 |
| | p2 | 2.65 | 2.70 | 2.56 | 2.40 | 2.69 | 2.72 | 2.63 | 2.61 | 2.74 |
| | p3 | 2.65 | 2.58 | 2.69 | 2.74 | 2.81 | 2.77 | 2.72 | 2.78 | 2.77 |
| | p4 | 3.09 | 3.28 | 3.16 | 3.20 | 3.17 | 3.36 | 3.30 | 3.28 | 3.90 |

Note: p1, p2, p3, and p4 respectively represents the decades 1966–1975, 1976–1985, 1986–1995, and 1996–2005.

Our results indicate differing trends among models for the proportion of land area under drought in the U.S. Generally, differences in climate predictions among GCMs arise from variations in initial conditions, parameterizations, or assumptions on emissions.

However, individual models tend to perform best in some aspects than others. Because of this, we observe that known historical drought events are captured in some models and not in others. Our results highlight some of the major intensively and extensively dry periods observed in the recent past and are in agreement with analyses by previous authors. According to Cook et al. [51] for example, >50% of the conterminous U.S. land area was under incipient to severe drought (PDSI < 1.0) in the summer of 2002. Based on our calculations, 50% to 60% of CONUS land area was under drought for the summer months of 2002. In 2011–2012, a major drought in the U.S. was termed the most severe on record [52], resulting in billions of dollars in economic losses [53]. From our results in Figure 1, it is observed that for IPSL, ACCESS, BCC, CCSM4, CMCC, and FGOALS, drier conditions began slightly after year 2011. Given that 2011 is the first computation year for the near-term to projected period, this observation is expected considering the tendency of PDSI to lag emerging droughts by several months [54], and thus its inability to detect drought on time scales shorter than 12 months [34]. Even so, historical records show that drought conditions persisted through the years 2013, 2014, and 2015 in some parts of the U.S., which may explain the protracted droughts indicated by IPSL, BCC, CCSM4, CMCC, MPI, and FGOALS for the period (Figure 2). In Figure 3a, major past dry spells are highlighted, confirming that our data and methods reproduce historical records. A recent dry period that began in 2012 is captured in Figure 3b. This has widely been documented as one of the most severe and extensive droughts in the USA [55,56].

At a time when IPCC projections indicate intensification of dry conditions in the subtropical areas of southern North America and expansion poleward [57], knowledge of spatial and temporal trends of projected drought is critical for resource planning in order to avoid surprises in the future. According to our analysis, the trend in percentage of land area under severe drought is expected to rise steadily until the year 2043, before briefly dropping in 2047, and then spiking again in 2050. Although the high-emissions scenario (RCP 8.5) assumed in this analysis will tend to indicate elevated drought conditions, relative comparison of the projected trend to past trend is a reliable way to understand the expectations. Considering the recent drought that occurred between 2012 and 2015, more prolonged drought over less land area would potentially occur beginning in the late 2030s to early 2040s. Severe drought would then be expected over more extensive areas approaching the year 2050. This information is highly valuable for strategic planning and management of critical resources such as water in terms of reservoir levels necessary for maintaining energy and food production over extended dry periods.

While several methods are available for clustering climate data, we elected to use a network-based method because it was within the framework in which we can characterize the topology of spatial drought heterogeneity. Moreover, the network-based community detection algorithm accommodates the use of edge weights and is efficient for dense networks. At a threshold of correlation coefficient >0.9, we discovered more stability in the spatial partitions and stronger cohesion within the clusters. Noting that spatial proximity among locations is not taken into consideration in the partitioning, it is not obvious that clusters would exhibit the geographic cohesion shown in Figure 6. The emergence of these clusters is indicative of localized spatial–temporal differences in climate, that can only be detected by using high-spatial-resolution climate data. Further characterization of such clusters is essential for the planning of local adaptation and mitigation strategies as well as understanding the spatial differences in land potential for various uses that depend on climate conditions such as urban ecological systems.

Our results must be interpreted keeping in mind the following limitations: available water capacity data used in the monthly PDSI computation are a constant value against a changing landscape; GCM data are an estimate and not an exact representation of the true climatic conditions; differences in GCM parameterizations yield disparate estimates of temperature and precipitation restricting comparability of subsequent derivatives, in this case PDSI; PDSI has known limitations that limit its validity for assessment of drought trends [58,59]. The main limitations relate to the Thornthwaite-based formulation for

estimating potential evaporation and its simplicity of the water balance model [58]. The Thornthwaite method may be substituted with other methods such as the Blaney–Criddle Formula, which has been shown to produce PDSI values that correlate highly with those based on the Thornthwaite method. As part of our future studies, we intent to examine differences between PDSI computed from observation data and those computed from GCM data in order to assess and understand differences in model performance. Previous studies have shown that bias correction of GCM data results in better agreement among models [60]. Given the observed differences in spatial and temporal distribution of PDSI among models in the current study, we will also explore the implications of GCM data bias correction for PDSI and compare them to implications on the data itself (uncertainties and intermodal differences).

5. Conclusions

In the current paper, we present an assessment of past and projected drought conditions over the CONUS as measured using PDSI. Performance of the modeled data to reproduce past drought events significantly differs among the models. However, calculated temporal patterns highlight major past drought events but do not clearly show less severe dry spells. The spatial trend of drought through the studied historical period (1966–2005) indicated continued drying over a section of the southwestern CONUS region including parts of south California, south Nevada, and west Arizona. In other parts of the country, agreement among the models is limited to small areas with statistics matching among a few of the models. Spatial trends in the near-term through the projected period show some intensification in the rate of drying for the southwestern CONUS region, as indicated by results from six out of the nine model datasets used. The projected frequency of severe drought months per year appears to be highest between 2041 and 2050 and intensified within small geographical areas, with other areas expected to experience two to zero months of severe drought per year on average.

By allowing a complete hydrological accounting, PDSI permits the assessment of drought severity. Access to reliable information on expected drought is of the essence for effective management of surface water for continued energy and food production. The ability to assess drought at local scales is necessary for localized action planning for which coarse-resolution GCM data are not applicable. Inadequacy of observed climate data necessitates improvement of modeling techniques to aid the assessment of local climate characteristics for better decision-making. The current analysis has demonstrated the efficacy of high-spatial-resolution data for highlighting local heterogeneity in drought patterns.

Author Contributions: Conceptualization, O.A.O.; formal analysis, S.M.K.; writing—original draft preparation, S.M.K.; writing—review and editing, O.A.O. and S.M.K. All authors have read and agreed to the published version of the manuscript.

Funding: This research received no external funding.

Data Availability Statement: DOE will provide public access to these results of federally sponsored research in accordance with the DOE Public Access Plan (<http://energy.gov/downloads/doe-public-access-plan>).

Acknowledgments: This manuscript has been authored by UT-Battelle, LLC, under contract DE-AC05-00OR22725 with the U.S. Department of Energy (DOE). The U.S. government retains and the publisher, by accepting the article for publication, acknowledges that the U.S. government retains a non-exclusive, paid-up, irrevocable, worldwide license to publish or reproduce the published form of this manuscript, or allow others to do so, for U.S. government purposes. DOE will provide public access to these results of federally sponsored research in accordance with the DOE Public Access Plan (<http://energy.gov/downloads/doe-public-access-plan>). This research was sponsored by the U.S. Department of Energy, Biological, and Environmental Research, under contract DE-AC05-00OR22725 with UT-Battelle, LLC.

Conflicts of Interest: The authors declare no conflict of interest.

References

1. Harto, C.B.; Yan, Y.E.; Demissie, Y.K.; Elcock, D.; Tidwell, V.C.; Hallett, K.; Macknick, J.; Wigmosta, M.S.; Tesfa, T.K. *Analysis of Drought Impacts on Electricity Production in the Western and Texas Interconnections of the United States*; Argonne National Laboratory (ANL): Argonne, IL, USA, 2012.
2. Poch, L.; Conzelmann, G.; Veselka, T. *An Analysis of the Effects of Drought Conditions on Electric Power Generation in the Western United States*; Rep. DOE/NETL-2009/1365, Morgantown, WV; Argonne National Laboratory (ANL): Argonne, IL, USA, 2009.
3. Ray, R.L.; Fares, A.; Risch, E. Effects of Drought on Crop Production and Cropping Areas in Texas. *Agric. Environ. Lett.* **2018**, *3*, 170037. [[CrossRef](#)]
4. Zipper, S.C.; Qiu, J.; Kucharik, C.J. Drought effects on US maize and soybean production: Spatiotemporal patterns and historical changes. *Environ. Res. Lett.* **2016**, *11*, 94021. [[CrossRef](#)]
5. Mosley, L.M. Drought impacts on the water quality of freshwater systems; review and integration. *Earth-Sci. Rev.* **2015**, *140*, 203–214. [[CrossRef](#)]
6. Sylvester, L.M.; Omitaomu, O.A.; Parish, E.S. *Analyzing the Implications of Climate Data on Plant Hardiness Zones for Green Infrastructure Planning: Case Study of Knoxville, Tennessee and Surrounding Region*; Oak Ridge National Laboratory (ORNL): Oak Ridge, TN, USA, 2016.
7. Wang, W.; Ertsen, M.W.; Svoboda, M.D.; Hafeez, M. Propagation of drought: From meteorological drought to agricultural and hydrological drought. *Adv. Meteorol.* **2016**, *2016*, 6547209. [[CrossRef](#)]
8. González-Hidalgo, J.C.; Vicente-Serrano, S.M.; Peña-Angulo, D.; Salinas, C.; Tomas-Burguera, M.; Beguería, S. High-resolution spatio-temporal analyses of drought episodes in the western Mediterranean basin (Spanish mainland, Iberian Peninsula). *Acta Geophys.* **2018**, *66*, 1–12. [[CrossRef](#)]
9. Cook, B.I.; Smerdon, J.E.; Seager, R.; Coats, S. Global warming and 21st century drying. *Clim. Dyn.* **2014**, *43*, 2607–2627. [[CrossRef](#)]
10. Huang, J.; Svoboda, M.; Wood, A.; Schubert, S.; Peters-Lidard, C.; Wood, E.; Pulwarty, R.; Mariotti, A.; Barrie, D.; United States National Oceanic and Atmospheric Administration; et al. *Research to Advance National Drought Monitoring and Prediction Capabilities*; National Oceanic and Atmospheric Administration: Washington, DC, USA, 2014; p. 28. [[CrossRef](#)]
11. Van Loon, A.F.; Stahl, K.; Di Baldassarre, G.; Clark, J.; Rangecroft, S.; Wanders, N.; Gleeson, T.; Van Dijk, A.I.J.M.; Tallaksen, L.M.; Hannaford, J.; et al. Drought in a Human-Modified World: Reframing Drought Definitions, Understanding, and Analysis approaches. *Hydrol. Earth Syst. Sci.* **2016**, *20*, 3631–3650. [[CrossRef](#)]
12. Dracup, J.A.; Lee, K.S.; Paulson, E.G. On the definition of droughts. *Water Resour. Res.* **1980**, *16*, 297–302. [[CrossRef](#)]
13. Wilhite, D.A.; Glantz, M.H. Understanding: The drought phenomenon: The role of definitions. *Water Int.* **1985**, *10*, 111–120. [[CrossRef](#)]
14. Tannehill, I.R. *Drought Its Causes and Effects*; Princeton University Press: Princeton, NJ, USA, 1947.
15. Hao, Z.; AghaKouchak, A.; Nakhjiri, N.; Farahmand, A. Global integrated drought monitoring and prediction system. *Sci. Data* **2014**, *1*, 1–10. [[CrossRef](#)]
16. Lu, L.; Yang, H.; Jonathan, L.; Rachel, R.; Bin, Y.; Zengxin, Z.; James, H.; Mark, S. Climatological Drought Analyses and Projection Using SPI and PDSI: Case Study of the Arkansas Red River Basin. *J. Hydrol. Eng.* **2013**, *18*, 809–816. [[CrossRef](#)]
17. Duffy, P.B.; Brando, P.; Asner, G.P.; Field, C.B. Projections of future meteorological drought and wet periods in the Amazon. *Proc. Natl. Acad. Sci. USA* **2015**, *112*, 13172–13177. [[CrossRef](#)] [[PubMed](#)]
18. Barker, L.J.; Hannaford, J.; Chiveron, A.; Svensson, C. From meteorological to hydrological drought using standardised indicators. *Hydrol. Earth Syst. Sci.* **2016**, *20*, 2483–2505. [[CrossRef](#)]
19. Spinoni, J.; Barbosa, P.; Bucchignani, E.; Cassano, J.; Cavazos, T.; Christensen, J.H.; Christensen, O.B.; Coppola, E.; Evans, J.; Geyer, B.; et al. Future global meteorological drought hot spots: A study based on CORDEX data. *J. Clim.* **2020**, *33*, 3635–3661. [[CrossRef](#)]
20. Steinhäuser, K.; Chawla, N.V.; Ganguly, A.R. Complex Networks In Climate Science: Progress, Opportunities And Challenges. In Proceedings of the CIDU, Mountain View, CA, USA, 5–6 October 2010; pp. 16–26.
21. Tsonis, A.A.; Swanson, K.L. Topology and predictability of El Nino and La Nina networks. *Phys. Rev. Lett.* **2008**, *100*, 228502. [[CrossRef](#)] [[PubMed](#)]
22. Tirabassi, G.; Masoller, C. Unravelling the community structure of the climate system by using lags and symbolic time-series analysis. *Sci. Rep.* **2016**, *6*, 29804. [[CrossRef](#)]
23. Scarsoglio, S.; Laio, F.; Ridolfi, L. Climate dynamics: A network-based approach for the analysis of global precipitation. *PLoS ONE* **2013**, *8*, e71129. [[CrossRef](#)]
24. Vejmelka, M.; Pokorná, L.; Hlinka, J.; Hartman, D.; Jajcay, N.; Paluš, M. Non-random correlation structures and dimensionality reduction in multivariate climate data. *Clim. Dyn.* **2015**, *44*, 2663–2682. [[CrossRef](#)]
25. Fan, J.; Meng, J.; Ashkenazy, Y.; Havlin, S.; Schellnhuber, H.J. Network analysis reveals strongly localized impacts of El Niño. *Proc. Natl. Acad. Sci. USA* **2017**, *114*, 7543–7548. [[CrossRef](#)]
26. Tupikina, L.; Rehfeld, K.; Molkenhain, N.; Stolbova, V.; Marwan, N.; Kurths, J. Characterizing the evolution of climate networks. *Nonlinear Process. Geophys.* **2014**, *21*, 705–711. [[CrossRef](#)]
27. Donges, J.F.; Schultz, H.C.H.; Marwan, N.; Zou, Y.; Kurths, J. Investigating the topology of interacting networks. *Eur. Phys. J. B* **2011**, *84*, 635–651. [[CrossRef](#)]
28. Fountalis, I.; Bracco, A.; Dovrolis, C. Spatio-temporal network analysis for studying climate patterns. *Clim. Dyn.* **2014**, *42*, 879–899. [[CrossRef](#)]

29. Palmer, W.C. *Meteorological Drought*; US Department of Commerce: Washington, DC, USA, 1965; p. 58.
30. Naz, B.S.; Kao, S.-C.; Ashfaq, M.; Rastogi, D.; Mei, R.; Bowling, L.C. Regional hydrologic response to climate change in the conterminous United States using high-resolution hydroclimate simulations. *Glob. Planet. Chang.* **2016**, *143*, 100–117. [[CrossRef](#)]
31. Jacobi, J.; Perrone, D.; Duncan, L.L.; Hornberger, G. A tool for calculating the palmer drought indices. *Water Resour. Res.* **2013**, *49*, 6086–6089. [[CrossRef](#)]
32. Thornthwaite, C.W. An approach toward a rational classification of climate. *Geogr. Rev.* **1948**, *38*, 55–94. [[CrossRef](#)]
33. Yuan, S.; Quiring, S.M. Drought in the U.S. Great Plains (1980–2012): A sensitivity study using different methods for estimating potential evapotranspiration in the Palmer Drought Severity Index. *J. Geophys. Res. Atmos.* **2014**, *119*, 911–996. [[CrossRef](#)]
34. Dai, A. The Climate Data Guide: Palmer Drought Severity Index (PDSI). Available online: <https://climatedataguide.ucar.edu/climate-data/palmer-drought-severity-index-pdsi> (accessed on 1 September 2021).
35. Mann, H.B. Nonparametric tests against trend. *Econom. J. Econom. Soc.* **1945**, *13*, 245–259. [[CrossRef](#)]
36. Yadav, R.; Tripathi, S.K.; Pranuthi, G.; Dubey, S.K. Trend analysis by Mann-Kendall test for precipitation and temperature for thirteen districts of Uttarakhand. *J. Agrometeorol.* **2014**, *16*, 164.
37. Pohlert, T. trend: Non-Parametric Trend Tests and Change-Point Detection. 2020. Package Version 1.1.4. Available online: <https://CRAN.R-project.org/package=trend> (accessed on 7 September 2021).
38. Theil, H. A rank-invariant method of linear and polynomial regression analysis. In *Henri Theil's Contributions to Economics and Econometrics*; Springer: Dordrecht, The Netherlands, 1992; pp. 345–381.
39. Sen, P.K. Estimates of the regression coefficient based on Kendall's tau. *J. Am. Stat. Assoc.* **1968**, *63*, 1379–1389. [[CrossRef](#)]
40. Tsonis, A.A.; Roebber, P.J. The architecture of the climate network. *Phys. A Stat. Mech. Appl.* **2004**, *333*, 497–504. [[CrossRef](#)]
41. Steinhäuser, K.; Chawla, N.V.; Ganguly, A.R. Complex networks as a unified framework for descriptive analysis and predictive modeling in climate science. *Stat. Anal. Data Min. ASA Data Sci. J.* **2011**, *4*, 497–511. [[CrossRef](#)]
42. Donges, J.F.; Zou, Y.; Marwan, N.; Kurths, J. Complex networks in climate dynamics. *Eur. Phys. J. Spec. Top.* **2009**, *174*, 157–179. [[CrossRef](#)]
43. Steinbach, M.; Tan, P.-N.; Kumar, V.; Klooster, S.; Potter, C. Discovery of Climate Indices Using Clustering. In Proceedings of the Ninth ACM SIGKDD International Conference on Knowledge Discovery and Data Mining, Washington, DC, USA, 24–27 August 2003; pp. 446–455. [[CrossRef](#)]
44. Newman, M.E.J.; Girvan, M. Finding and evaluating community structure in networks. *Phys. Rev. E* **2004**, *69*, 26113. [[CrossRef](#)] [[PubMed](#)]
45. Blondel, V.D.; Guillaume, J.L.; Lambiotte, R.; Lefebvre, E. Fast unfolding of communities in large networks. *J. Stat. Mech. Theory Exp.* **2008**, *2008*, P10008. [[CrossRef](#)]
46. Moon, H.; Gudmundsson, L.; Seneviratne, S.I. Drought persistence errors in global climate models. *J. Geophys. Res. Atmos.* **2018**, *123*, 3483–3496. [[CrossRef](#)]
47. Dai, A. Drought under global warming: A review. *Wiley Interdiscip. Rev. Clim. Chang.* **2011**, *2*, 45–65. [[CrossRef](#)]
48. Dai, A. Increasing drought under global warming in observations and models. *Nat. Clim. Chang.* **2013**, *3*, 52. [[CrossRef](#)]
49. Dai, A.; Trenberth, K.E.; Qian, T. A global dataset of Palmer Drought Severity Index for 1870–2002: Relationship with soil moisture and effects of surface warming. *J. Hydrometeorol.* **2013**, *5*, 1117–1130. [[CrossRef](#)]
50. Dai, A. Dai Global Palmer Drought Severity Index (PDSI). Research Data Archive at the National Center for Atmospheric Research, Computational and Information Systems Laboratory. 2017. Available online: <https://doi.org/10.5065/D6QF8R93> (accessed on 7 September 2021).
51. Cook, E.R.; Seager, R.; Heim, R.R., Jr.; Vose, R.S.; Herweijer, C.; Woodhouse, C. Megadroughts in North America: Placing IPCC projections of hydroclimatic change in a long-term palaeoclimate context. *J. Quat. Sci.* **2010**, *25*, 48–61. [[CrossRef](#)]
52. Peterson, T.C.; Stott, P.A.; Herring, S. Explaining extreme events of 2011 from a climate perspective. *Bull. Am. Meteorol. Soc.* **2012**, *93*, 1041–1067. [[CrossRef](#)]
53. Fannin, B. Updated 2011 Texas agricultural drought losses total \$7.62 billion. In *AgriLife Today*; Texas A&M AgriLife Extension: College Station, TX, USA, 2011; Available online: <https://agrifetoday.tamu.edu/2012/03/21/updated-2011-texas-agricultural-drought-losses-total-7-62-billion/> (accessed on 7 September 2021).
54. Alley, W.M. The Palmer Drought Severity Index: Limitations and Assumptions. *J. Clim. Appl. Meteorol.* **1984**, *23*, 1100–1109. [[CrossRef](#)]
55. NOAA National Centers for Environmental Information State of the Climate: Drought for June 2012. NOAA National Centers for Environmental Information. 2012. Available online: <https://www.ncdc.noaa.gov/sotc/drought/201207> (accessed on 7 September 2021).
56. Rippey, B.R. The US drought of 2012. *Weather Clim. Extrem.* **2015**, *10*, 57–64. [[CrossRef](#)]
57. Intergovernmental Panel on Climate Change. “Climate Change 2007: The Physical Science Basis”. Agenda 6, no. 07. 2007. Available online: https://www.slvwd.com/sites/g/files/vyhlf1176/f/uploads/item_10b_4.pdf (accessed on 7 September 2021).
58. Burke, E.J. Understanding the sensitivity of different drought metrics to the drivers of drought under increased atmospheric CO₂. *J. Hydrometeorol.* **2011**, *12*, 1378–1394. [[CrossRef](#)]

-
59. Sheffield, J.; Wood, E.F.; Roderick, M.L. Little change in global drought over the past 60 years. *Nature* **2012**, *491*, 435. [[CrossRef](#)] [[PubMed](#)]
 60. Troin, M.; Velázquez, J.A.; Caya, D.; Brissette, F. Comparing statistical post-processing of regional and global climate scenarios for hydrological impacts assessment: A case study of two Canadian catchments. *J. Hydrol.* **2015**, *520*, 268–288. [[CrossRef](#)]